Neural Computing and Applications (2020) 32:14019–14029
https://doi.org/10.1007/s00521-020-04801-1

ORIGINAL ARTICLE

Fuzzy association rule-based set-point adaptive optimization and control for the flotation process

Mingxi Ai[1] · Yongfang Xie[1] · Shiwen Xie[1] · Jin Zhang[1] · Weihua Gui[1]

Received: 19 May 2019 / Accepted: 17 February 2020 / Published online: 5 March 2020
© Springer-Verlag London Ltd., part of Springer Nature 2020

Abstract
Froth flotation is a complicated process which is difficult to establish its first-principle model. Due to the fluctuations in the grade of raw ore, adaptively adjusting the set-points is extremely important in the flotation process. The inappropriate set-points easily lead to the instability of the process. This paper presents a fuzzy association rule-based set-point adaptive optimization and control strategy for the antimony flotation process without knowing the system model. Firstly, a fuzzy neural network is constructed as a soft-sensor to estimate the feed grade online because of the lack of efficient measurement equipment. Then, fuzzy association rule is used to mine the hidden relationship between the feed grade with reagent dosages and the optimal set-points. Through data mining from the quantitative database, the fuzzy inference system generates the optimal set-points. To implement satisfactory tracking performance, predictive controller is used to compute the control inputs. Because the system dynamics is unknown, long short-term memory network model is established to predict the future behaviors of the process. Finally, simulations and experiments are carried out to demonstrate the effectiveness of the proposed strategy. Compared to the manual manipulation, which is widely used in flotation processes, our control strategy achieves a better control performance, and the concentrate grades are more in line with the process requirement.

Keywords Fuzzy neural network · Fuzzy association rule · Set-point optimization · Predictive control · Flotation process

1 Introduction

A general industrial process control scheme usually involves an optimization module which generates the set-points of the operational indices that maximize the economic performance function, and a controller which tracks the set-points [1–3]. A case in point is the froth flotation which is an important mineral concentration technique. The flotation is a complicated process with nonlinear dynamic behavior and uncertainty. The grade of the raw ore and prices of the reagents vary with the market, such that the set-points for the lower-level controller should be adjusted corresponding to the feed conditions. The set-points of the operational indices are related to the optimal operation of the flotation process. Studies [1–3] pointed out that predictive models of the operational indices are important to calculate the optimal set-points. For the flotation processes, however, it is difficult to build its first-principle model, resulting in the challenges in the optimization of the set-points. It is widely accepted that the appearance features are good indicators that characterize the operational performance of the flotation processes [4–8]. Hence, in most flotation plants, the process is controlled by manually observing the appearance of the froth surface. For example, the froth appearance features include bubble size, bubble shape, color, and texture. The study in [6] illustrated the froth features can be viewed as numerical estimates of froth status or health, and then, a new way for modeling of flotation processes was presented based on the froth appearances. In [7], a union distribution of the bubble size and bubble shape was proposed to describe the froth image features. Then, a data-driven model was built to predict the future froth appearances. To reveal the mapping between the working conditions and the froth appearance, neural networks were used to model the batch flotation

✉ Shiwen Xie
sw.xie@csu.edu.cn

[1] School of Automation, Central South University, Changsha 410083, Hunan, China

www.manaraa.com

process with the froth image features as the input variables [8].

From the previous studies, we know that appropriate froth image features imply the good control performance of the flotation process. However, how to determine the appropriate values of the features is a challenge for the flotation processes. For a simple system, the set-point is easy to be determined, or a fixed set-point is enough. In the optimization of industrial processes, many studies concern on the set-point optimization method. In [9], an adaptive steady-state target optimization was designed to calculate online optimal set-points for model predictive control (MPC). It maximizes economic profits to obtain the optimal set-point. In the operation of the wastewater treatment plant, the real-time optimization (RTO) was presented in the upper layer to obtain the optimal target [10]. In this study, both static RTO and dynamic RTO were used in response to the steady-state and dynamic processes. For the control of the networked flotation processes, optimization layer was constructed to provide the set-point for the robust MPC [11]. In [12], off-policy Q-learning method was proposed to find the optimal set-points using measured data for the rougher flotation operational processes. In [11, 12], they tried to find the set-points of the system outputs, such as concentrate grade and tail concentrate. So far, few studies concern on calculating the optimal froth image feature to guide the manipulation of the flotation process. Though this question has been realized for a long time, most of the computer-vision-based researches use the expert experience to set optimal image features. Recently, Xie et al. [13] tried to link the set-points with feed grade using clustering method. In this method, the feed grade was classified to different clusters offline, and the optimal surface bubble behavior for each cluster was set manually in advance. In the historical data of the flotation processes, abundant association knowledge between the feed grade with previous control inputs and the optimal froth image features is hidden. Association rule mining is an effective technique to dig out the association rule [14–18]. The goal of association rule mining is to discover important associations among items such that the presence of some items in a transaction will imply the presence of some other items. In [19], two fuzzy association rule (FAR) mining models were investigated for enhancing prediction performance. The FARs is utilized to provide the knowledge base for the prediction evaluation of fuzzy inference system. In misuse detection application, fuzzy grids-based association rules mining was presented for feature selection [20]. In [21], a fuzzy logic controller was designed based on FARs for the mineral processing. The FARs was used to find some uncovered relationships. In the zinc froth flotation process, FAR was introduced to association rule between the working conditions and the optimal froth surface behavior features [22]. To our best knowledge, few studies investigate the optimization of set-point using the FAR. Therefore, studying how to mine the association rule between the feed conditions and the optimal froth image feature is still a tough problem in the control of the flotation process.

Subsequent to the optimization, control method design is the third challenge for the flotation process. In the control community, many control techniques have been proposed, such as PID [23], fuzzy PID [24], predictive control [25], fuzzy control [26], optimal control [27], and robust control [28]. Wu et al. [29, 30] proposed a novel optimal sliding mode control method for complex hybrid systems, which has strong robustness to the external uncertainties, thus can be utilized to the flotation process considered in this work; also, with such an optimal sliding mode control, the transient performance of the controlled system has been greatly improved. Predictive control is one of the widely used control techniques in industrial processes [31]. Hence, we use the predictive control technique to deduce the optimal reagent dosages to implement the set-point tracking. In this paper, we propose a fuzzy association rule-based set-point adaptive optimization and control strategy for the antimony flotation process. The novelties of our paper lie on: (1) An FNN-based soft-sensor with dynamically adjusting the number of the fuzzy sets is developed to estimate the feed grade online; (2) FARs are constructed to generate the optimal set-points of the image features; (3) a long short-term memory network (LSTM) model is established to approximate the antimony flotation process, and then predictive controller is used to calculate the control inputs to track the set-points. Our proposed strategy is validated by the simulations and experiments in the real-world plant.

The remainder of this paper is organized as follows: Sect. 2 describes the process and the framework of the proposed strategy. The detailed implementation of the strategy is presented in Sect. 3. Simulations and experiments are shown in Sect. 4. Section 5 draws the conclusions.

2 Overall description of the proposed strategy

2.1 Process description

The flow diagram of an antimony flotation plant in China is shown in Fig. 1. Raw ore is firstly crushed and grinded into a fine powder by large rotating mills, and the latter is mixed with water and special reagents to form slurry. After the gold flotation process, the tailings from gold rougher bank are pumped to the antimony flotation procedure. The

www.manaraa.com

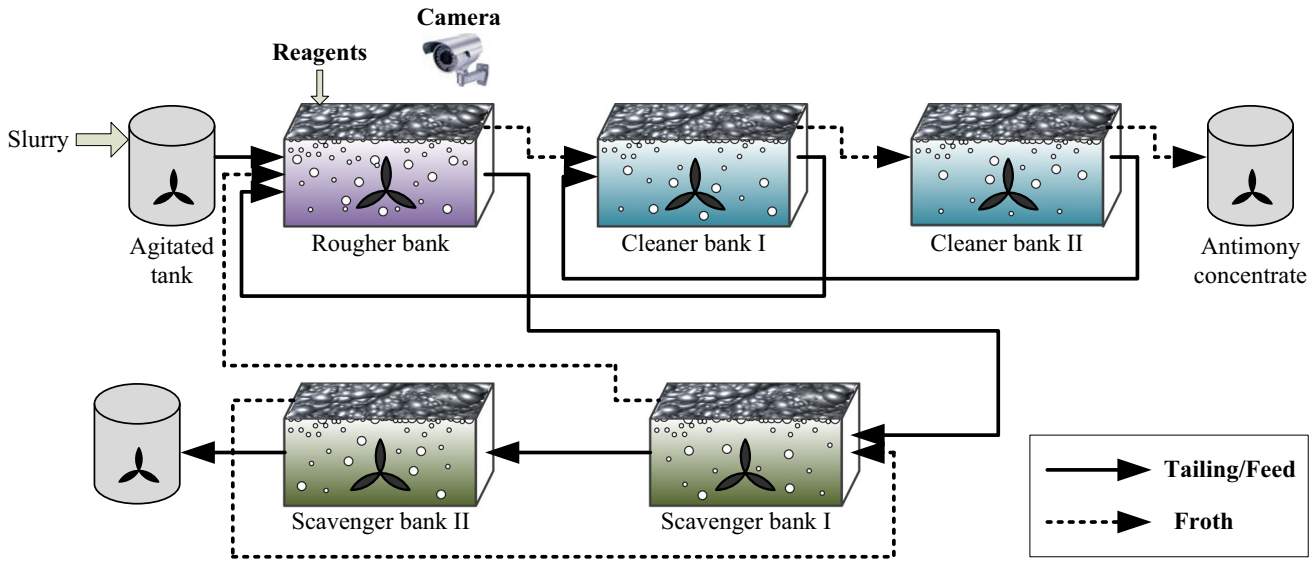

Fig. 1 Flow diagram of the antimony flotation process

antimony flotation is divided into several banks, including rougher bank, cleaner bank, and scavenger bank. The rougher bank is the first and most important step, because over 60% minerals are recovered in this bank. To make the antimony mineral particles separate from the useless materials, five kinds of reagents are injected to the rougher circuit. Foaming agent, including #2 oil, is used to stabilize foams; copper sulfate and lead nitrate are the activators which promote the reaction between the reagents and valuable minerals; collectors are used to change the mineral surface hydrophobicity, which include black powder and xanthate. With the action of the reagents, bubbles in the rougher circuit carry the mineral particles to the upper layer of the slurry, forming a froth layer. Then, the froths are delivered to cleaner banks to further extract and concentrate the valuable mineral. The slurry of the cleaner banks will be recycled to the rougher circuit. The lower layer of the slurry flows to the scavenger banks which are auxiliary to recover the mineral. Finally, we obtain the antimony concentrate from the cleaner banks.

Through observing the froth image, operators manipulate the reagent dosages to make the antimony concentrate grade in the desired range. In our case, it should be controlled around 32%, preferably in [31%, 33.5%]. The manual manipulation largely depends on operators' frequent observation and expert experience. The experience and motivational levels of operators vary substantially so that it easily causes excessive consumption of the reagents and process fluctuations, which affect final product quality and economic profit. To overcome the drawbacks of manual operation, we proposed the following strategy to implement the automatic control of the antimony flotation process.

2.2 Overall structure of the optimization and control strategy

A fuzzy association rule-based set-point optimization and LSTM-based predictive control strategy for the flotation process are proposed in this paper. The schematic of the proposed strategy is depicted in Fig. 2, and the variables in the figure are explained as follows:

x_1, x_2, x_3, x_4 Froth image features, bubble size, bubble shape, froth color, and froth velocity. $\boldsymbol{x} = [x_1, x_2, x_3, x_4]^{\mathrm{T}}$

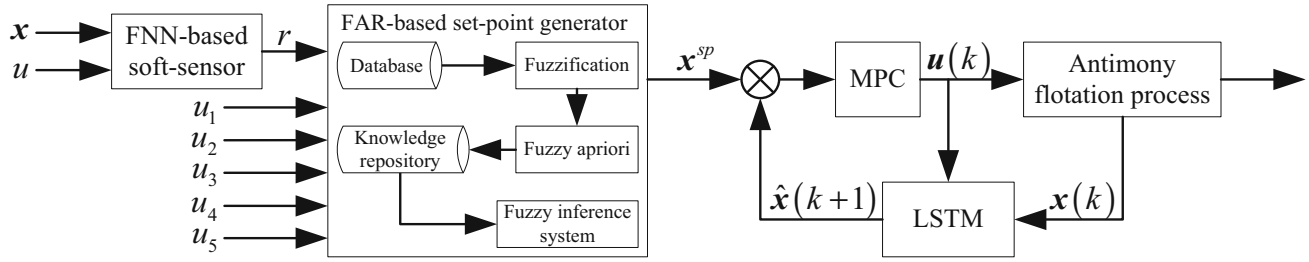

Fig. 2 Schematic of FAR-based set-point optimization and control strategy

www.manaraa.com

r	Feed grade
$\boldsymbol{x}^{\mathrm{sp}}$	Optimal set-point of the froth image feature, $\boldsymbol{x}^{\mathrm{sp}} = \left[x_1^{\mathrm{sp}}, x_2^{\mathrm{sp}}, x_3^{\mathrm{sp}}, x_4^{\mathrm{sp}}\right]^{\mathrm{T}}$
u_1, u_2, u_3, u_4, u_5	Reagent dosages, $\boldsymbol{u} = [u_1, u_2, u_3, u_4, u_5]^{\mathrm{T}}$

The strategy contains three submodules: an FNN-based soft-sensor, an FAR-based set-point generator, and an LSTM-based predictive controller. The descriptions of each module are presented as follows.

1. *FNN-based soft-sensor* The fluctuation of the feed grade is the major disturbance in the flotation process. The feed grade varies with the source of the raw ore and market, which is unpredictable. It influences the froth image features. Hence, the optimal set-points of the image features should be adjusted corresponding to the variation of the feed grade. However, the feed grade is usually measured by laboratory analysis. It is time-consuming, and worst of all, we cannot obtain this value in real time so as to adjust the set-points. Hence, FNN-based soft-sensor approach is used to estimate the feed grade online, because FNN has a good approximation ability and generalization performance [32, 33]. The inputs of the FNN are the current froth image features and reagent dosages. Bubble size, bubble shape, color, and velocity are chosen to characterize the froth appearance.
2. *FAR-based set-point generator* The fluctuation of the feed grade that results in the fixed set-points does not satisfy the control requirements. Inappropriate set-points make the controller difficult to implement a good tracking performance. It is of importance to find the relationship among the feed grade, reagent dosages, and optimal set-points of image features. In the flotation plant, a lot of production data, including the feed grade, reagent dosages, froth image, and concentrate grade, are generated every day, which provide us a basis to extract the implicit relationship. FARs can extract the hidden association patterns and the correlation between the items in the large database. Therefore, we employ FARs to generate the optimal set-points.
3. *LSTM-based predictive controller* A predictive model is crucial to the predictive controller. The mechanism process of the flotation is complicated so as to difficult to build its first-principle model. We use LSTM to model the antimony process, whose performance is established by our previous study [34]. Then, the predictive controller is constructed to calculate the control inputs to accomplish the set-points tracking.

It is noteworthy that the data used in FNN-based soft-sensor and FAR-based set-point generator are steady-state data. This is for the reason that reagents usually take about 5–10 min to change the hydrophobicity of minerals' surface. When the grade of feed slurry or other disturbance causes the fluctuation of flotation status, the flotation working condition is continuously changing. Thus, input images for the FNN-based soft-sensor and FAR-based set-point generator should be captured in a new stable status after fluctuation.

3 Realization of the proposed strategy

3.1 FNN-based soft-sensor

An online estimation of the feed grade is necessary to calculate the optimal set-points of the froth image features. Our previous research reported that the feed grade is a nonlinear function of the image features and reagent dosages [35]:

$$r = f_1(\boldsymbol{z}) \tag{1}$$

where r denotes the feed grade. $\boldsymbol{z} = [x_1, x_2, x_3, x_4, \boldsymbol{u}]^{\mathrm{T}}$ is the input vector. $f_1(\cdot)$ is an unknown nonlinear function, which is approximated by FNN. The network consists of five layers. Layer-1 is the input layer which transmits the inputs to the linguistic variables in the next layer.

Layer-2 is the fuzzification layer. Each node in this layer links several fuzzy sets. The output specifies the degree to which an input value belongs to a fuzzy set. Since Gauss membership function is the basis for the connection between fuzzy systems and radial basis function neural networks (RBFNN). Gauss membership function is utilized as the membership function:

$$\mu_i^j(z_i) = \exp\left[-\left(z_i - c_i^j\right)^2 \Big/ \left(\sigma_i^j\right)^2\right] \tag{2}$$

where $\exp(\cdot)$ denotes the exponential function. c_i^j and σ_i^j are the mean and standard deviation of the Gauss function in the jth node of the ith input variable, respectively.

Layer-3 is the rule antecedent layer, in which product fuzzy AND logic is used to calculate the firing strength:

$$\psi_m = \prod_{i=1}^{9} \mu_i^j(z_i) \tag{3}$$

where ψ_m is the mth output of the rule layer. The number of m is determined by the input number and fuzzy set number.

Layer-4 is the rule consequent layer. The output of this layer is the linear combination of the layer-3 and the connected weight ω_m.

Layer-5 is the defuzzification layer. The center of gravity defuzzification method [36] is used to obtain the final output.

www.manaraa.com

$$r = \sum_{m=1}^{M} \omega_m \psi_m \Big/ \sum_{m=1}^{M} \psi_m \tag{4}$$

The performance of the FNN relies on the well-defined set of parameters [37], including the centers and widths of the Gaussian functions, the number of the fuzzy sets, and the weights. A training algorithm with dynamically adjusting the number of the fuzzy sets is proposed to obtain the parameters. The implementation of the training procedures is presented as follows:

Step 1 Initialize parameters of the FNN.

Step 1-1 Using every kinds of image feature classifying flotation status into K typical classes. Correspondingly, there are K fuzzy sets for every kind of image feature. Mean and standard deviation of each class are calculated and used to initialize parameters of membership functions.

Step 1-2 The number of fuzzy sets and corresponding membership function parameters for reagents are set according to those frequently adopted reagent dosages in manual control.

Step 1-3 Initialize ω_m using the normal distribution (mean = 0, std = 1).

Step 2 For the training data $\{z(l), \hat{y}(l)\}$, in which $\hat{y}(l)$ is the measured feed grade of the lth sample, calculate the estimation of the FNN. The predictive error $e(l)$ is $\hat{y}(l) - r(l)$.

If $|\hat{y}(l) - r(l)| \le \varepsilon_1$ (ε_1 is an error threshold), go to step 4, otherwise go to next step.

Step 3 For all the input variables $z_i(l)$, verify it belongs to the effective range of the current Gaussian functions or not.

If $\frac{\left(z_i(l) - c_i^j\right)^2}{\left(\sigma_i^j\right)^2} \ge \xi_j^2$, then add a new fuzzy set for the ith input. The center of the new Gaussian function is $z_i(l)$, and the new width and weight are selected randomly.

Else use gradient descent algorithm to tune the parameters $\boldsymbol{\theta}^{\text{new}} = \boldsymbol{\theta} - \eta \frac{\partial E(l)}{\partial \boldsymbol{\theta}}$, where $\boldsymbol{\theta} = \left[c_i^j, \sigma_i^j, \omega_m\right]^{\mathrm{T}}$. $E(l)$ is the cost function, $E(l) = \frac{1}{2}(\hat{y}(l) - r(l))^2$. η denotes the learning rate.

Step 4 $l = l + 1$, go to step 2 until the maximum number of the training data.

Step 5 Use cross-validation method to test the performance of the FNN.

It is noteworthy that the gradient descent is a generic method for continuous optimization and is very commonly applied to nonconvex functions. With a smooth function $E(l)$ and a reasonably learning rate η, it will generate a sequence of points with strictly decreasing values of the cost function. Gradient descent will eventually converge to a stationary point of the function, regardless of convexity. If the function is nonconvex, a local minimizer is found.

3.2 FAR-based set-point generator

In the antimony flotation plant, numerous production data are produced every day, which imply the relationship among the feed grade, reagent dosages, and optimal set-points of image features. We use FAR to mine the interesting and potentially useful regularities. The FAR can be presented in the form of IF X Then Y, indicating that if the items in X exist in a transaction, then the items in Y are also in this transaction with a high probability. To generate the set-points, the FAR is described as:

R_n: IF x_1 is A_{1n} and x_2 is A_{2n} and x_3 is A_{3n} and x_4 is A_{4n} and x_5 is A_{5n} and r is A_{6n}
THEN x_1^{sp} is B_{1n} and x_2^{sp} is B_{2n} and x_3^{sp} is B_{3n} and x_4^{sp} is B_{4n}

where $A_{in}(i = 1, \ldots, 6)$ and $B_{jn}(j = 1, \ldots, 4)$ are the fuzzy sets for the antecedent and consequent linguistic terms, respectively. The number of the rules is determined by the number of the fuzzy sets, and the latter is determined by the expert experience. Different expert, however, has different experiences, resulting in the uncertainties in the FAR. In this study, therefore, Gaussian membership functions with a fixed standard deviation and an uncertain mean are introduced for each linguistic term, shown in Fig. 3. The number of membership functions and their parameters for each input are determined empirically. Generally, the FAR mining process can be divided into two phases. First, the transaction data are scanned to calculate the frequency of each linguistic term. If the frequency of an item in the transactions is larger than a predefined threshold value (called minimum support, denoted by *minsup*), we consider that it is a large item. In the second phase, the strong association rules are generated from the large itemsets. The detailed procedures are summarized as follows:

Step 1 For the given transaction data $\boldsymbol{D}^{(l)}$ ($\left\{z_i^{(l)}, 1 \le l \le M\right\}$), transform the quantitative input $z_i^{(l)}$

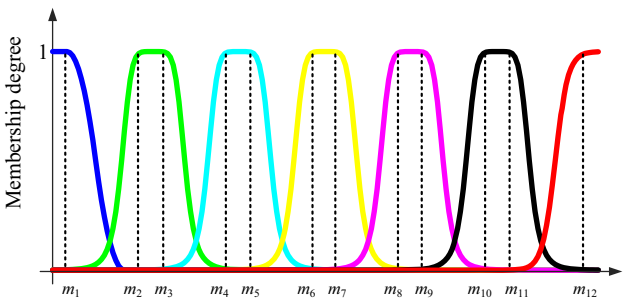

Fig. 3 Fuzzy membership functions

www.manaraa.com

into fuzzy sets using the Gaussian membership functions, described as:

$$\left\{\frac{f_{i1}^{(l)}}{R_{i1}}+\frac{f_{i2}^{(l)}}{R_{i2}}+\cdots+\frac{f_{iN}^{(l)}}{R_{iN}}\right\} \tag{5}$$

where $R_{in}(n=1,\ldots,N)$ is the nth fuzzy region of the ith input data. $f_{in}^{(l)}$ is the fuzzy membership degree in the region R_{in} for the lth sample.

Step 2 Calculate the support value for each fuzzy region using the following equation:

$$Support_{in}=\sum_{l=1}^{M} f_{in}^{(l)} \tag{6}$$

Step 3 For each R_{in}, if $Support_{in}\geq minsup$, put it in the set of large itemsets L_1. That is

$$L_1=\{R_{in}|Support_{in}\geq minsup,\quad 1\leq i\leq 10,\quad 1\leq n\leq N\} \tag{7}$$

Step 4 Let r represent the number of items in the current large itemsets, and its initial value is 1. Combine the large itemsets L_r to generate new candidate set C_{r+1}. It is worth noting that two fuzzy regions belonging to the same attribute cannot be added to the same candidate set simultaneously.

Step 5 For the newly formed set C_{r+1}, we assume that there $r+1$ linguistic terms, denoted as a_1, $a_2,\ldots,a_{r+1}$. Calculate the fuzzy value of each terms using minimum operator:

$$\mu_a=\mu_{a_1}\wedge\mu_{a_2}\wedge\cdots\wedge\mu_{a_{r+1}} \tag{8}$$

Step 6 Calculate the support value of the candidate set. If the support is equal or greater than *minsup*, then move this itemset to L_{r+1}.

Step 7 Let $r=r+1$, and repeat steps 5–7 until there are no available combinations to be found.

Step 8 Collect the frequent itemsets together. For each large itemset L_{r+1}, generate all the possible association rules as the form of IF–Then.

Step 9 Calculate the confidence value (CV) of each association rule:

$$CV=\frac{\sum[(\mathrm{IF})\cap(\mathrm{Then})]}{\sum(\min(\mathrm{IF}))} \tag{9}$$

Step 10 Only keep the association rules that their CVs are equal or greater than the predefined threshold value.

After determining the association rules, we use fuzzy inference system to generate the set-points of the froth image features. We assume that P association rules have been obtained. The strength for the pth rule is computed by:

$$\phi(p)=\min\left\{\mu_{A_{p1}}(z_1),\mu_{A_{p2}}(z_2),\ldots,\mu_{A_{p6}}(z_6)\right\} \tag{10}$$

where $\mu_{A_{pi}}(z_i)$ denotes the truth value of the input z_i in the pth rule. Let b_p^j $(j=1,\ldots,4)$ denotes the resulting fuzzy control value for the jth output of the pth rule. Then, the crisp output of the FAR is

$$x_j^{\mathrm{sp}}=\frac{\sum_{p=1}^{P}\phi(p)b_p^j}{\sum_{p=1}^{P}\phi(p)}. \tag{11}$$

3.3 LSTM-based predictive controller

In this section, we aim to implement the tracking control of the set-points of the froth image feature. The predictive controller is constructed to accomplish this task, described as

$$\begin{aligned}
&J(k)=\sum_{h=1}^{T_p}[\boldsymbol{x}^{\mathrm{sp}}(k+h)-\hat{\boldsymbol{x}}(k+h)]^2+\lambda\sum_{h=0}^{T_u}\Delta\boldsymbol{u}^2(k+h)\\
&\text{s.t.}\,\hat{\boldsymbol{x}}(k+1)=f_2(\boldsymbol{x}(k),\boldsymbol{u}(k))\\
&\quad\boldsymbol{x}_{\min}\leq\hat{\boldsymbol{x}}(k)\leq\boldsymbol{x}_{\max}\\
&\quad\boldsymbol{u}_{\min}\leq\boldsymbol{u}(k)\leq\boldsymbol{u}_{\max}\\
&\quad\Delta\boldsymbol{u}_{\min}\leq\Delta\boldsymbol{u}(k)\leq\Delta\boldsymbol{u}_{\max}
\end{aligned} \tag{12}$$

where $\hat{\boldsymbol{x}}(k)$ denotes the predicted froth image feature vector at discrete sampling instant k, which is restricted in $[\boldsymbol{x}_{\min},\boldsymbol{x}_{\max}]$. $f_2(\cdot)$ is an unknown nonlinear mapping function. λ is a weight. T_{p} and T_{u} are the prediction horizon and control prediction horizon, respectively. $\boldsymbol{u}_{\min}$ and $\boldsymbol{u}_{\max}$ are the lower and upper bounds of $\boldsymbol{u}(k)$. $\Delta\boldsymbol{u}(k)=\boldsymbol{u}(k)-\boldsymbol{u}(k-1)$, which should be limited in $[\Delta\boldsymbol{u}_{\min},\Delta\boldsymbol{u}_{\max}]$.

For the predictive controller, an effective system model is critical to its control performance. It is widely accepted that the flotation processes are difficult to establish the first-principle model [38, 39]. Therefore, we use LSTM to identify the nonlinear function $f_2(\cdot)$ because of its good performance on sequential data [34]. The LSTM can be formulated as:

$$\begin{aligned}
\mathbf{c}^+&=\sigma_{\mathrm{s}}(\mathbf{W}_{\mathrm{f}}\boldsymbol{\chi}+\mathbf{U}_{\mathrm{f}}\mathbf{h}+\mathbf{b}_{\mathrm{f}})\circ\mathbf{c}\\
&\quad+\sigma_{\mathrm{t}}(\mathbf{W}_i\boldsymbol{\chi}+\mathbf{U}_{\mathrm{i}}\mathbf{h}+\mathbf{b}_{\mathrm{i}})\circ\sigma_{\mathrm{s}}(\mathbf{W}_{\mathrm{c}}\boldsymbol{\chi}+\mathbf{U}_{\mathrm{c}}\mathbf{h}+\mathbf{b}_{\mathrm{c}})\\
\mathbf{h}^+&=\sigma_{\mathrm{t}}(\mathbf{W}_{\mathrm{h}}\boldsymbol{\chi}+\mathbf{U}_{\mathrm{h}}\mathbf{h}+\mathbf{b}_{\mathrm{h}})\circ\sigma_{\mathrm{s}}(\mathbf{c}^+)\\
\mathbf{x}^+&=\mathbf{W}_{\mathrm{o}}\cdot\mathbf{h}^+\mathbf{b}_{\mathrm{o}}
\end{aligned} \tag{13}$$

where $\boldsymbol{\chi}=[\mathbf{x}^{\mathrm{T}}\ \mathbf{u}^{\mathrm{T}}]$, $\boldsymbol{c}$ is internal memory cell state, and $\boldsymbol{h}$ is hidden state. $\boldsymbol{x}^+$ indicates the value of $\boldsymbol{x}$ at the next time step, i.e., $\mathbf{x}(k+1)$. $\sigma_{\mathrm{s}}(x)=\frac{1}{1+\mathrm{e}^{-x}}$ and $\sigma_t(x)=\tanh(x)$. $\circ$ is the elementwise product. The terms $\boldsymbol{W}_{\mathrm{f}}$, $\boldsymbol{W}_{\mathrm{i}}$, $\boldsymbol{W}_{\mathrm{c}}$, $\boldsymbol{W}_{\mathrm{h}}$, $\boldsymbol{W}_{\mathrm{o}}$,

www.manaraa.com

$\boldsymbol{U}_f$, $\boldsymbol{U}_i$, $\boldsymbol{U}_c$, $\boldsymbol{U}_h$ are weighting matrices, and $\boldsymbol{b}_f$, $\boldsymbol{b}_i$, $\boldsymbol{b}_c$, $\boldsymbol{b}_h$, $\boldsymbol{b}_o$ are biasing vectors. The weights and bias are offline learned using the historical data.

4 Experiments and results

To evaluate the performance of our proposed control strategy, industrial experiments were carried out at an antimony flotation plant in China. In the antimony flotation plant, our research team has developed a machine vision-based monitor platform using an industrial RGB camera. The software systems, programmed by Microsoft Visual C ++ and MATLAB, analyze the images and extract froth image features. Four kinds of image features, containing bubble size, bubble shape, froth velocity, and froth color, are used in this study.

1. To obtain the bubble size feature, the froth images are segmented by a marker watershed method. To identify high-light spot (marker) on the top of bubbles, H-minimal transform is used to explore the basins with depth greater than a predefined threshold h for each individual bubble. After setting markers as local minimal regions in the complement image, watershed transform is performed to obtain the segmentation result [40]. An example is shown in Fig. 4a.
2. After watershed image segmentation, individual bubbles are labeled as different connected components. The diameter of the maximal inscribed circle and circumcircle of each individual bubble are calculated. The bubble shape is characterized as the following average aspect ratio:

$$R = \frac{1}{n}\sum_{i=1}^{n}\frac{a_i}{b_i} \tag{14}$$

where a is the diameter of the maximal inscribed circle and b is the diameter of the circumcircle [41].
3. To extract froth color, the RGB froth image is firstly transformed to HSV color space. Then, the average value of H-channel is calculated and used as the froth color feature.
4. Froth velocity is used to capture the dynamic behavior of the froth and can be quantified by tracking the froth movement in two consecutive frames by registering key points in a fixed size image block. Firstly, a block consisting of N_{row} columns in the left of the first frame is selected (denoted as $B_{reference}$). Then, a series of continuous N_{row} columns-sized blocks in the next frame are extracted. In these blocks, the ith block (B^i_{detect}) represents a block starts at column i. ORB (Oriented FAST and Rotated BRIEF) is introduced to do key points registration between $B_{reference}$ and B^i_{detect}. The image block that has the highest matching score is used as the matching block, and its column index is known as instantaneous speed [22]. An image block matching using key point registration is shown in Fig. 4b. Ten consecutive video frames are registered, and their average instantaneous speed is used as the froth velocity feature. According to the test time for feature extraction, about 11 s (specifically, 0.867 s for bubble size and shape, 10.041 s for one set of froth velocity, 0.0161 s for froth color) were enough in our computer (Core i7-7800X, 32G RAM).

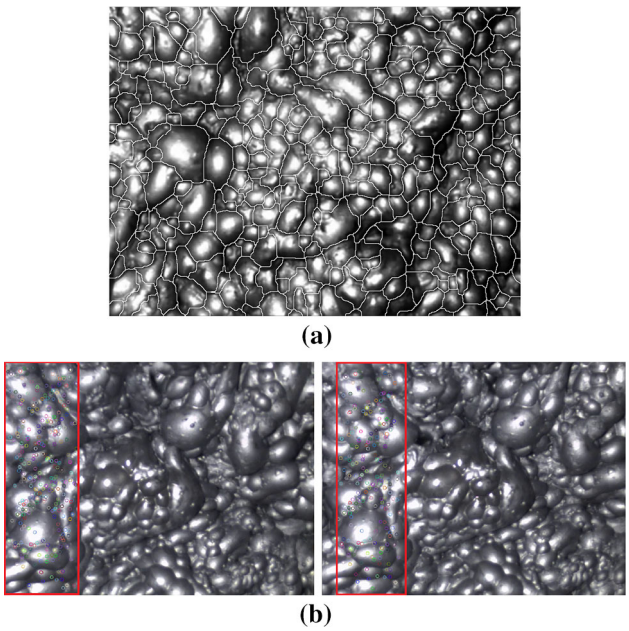

Fig. 4 Image feature extraction. **a** Segmentation results; **b** froth block matching by key points registration

Then, we conducted simulations to verify the effectiveness of the FNN-based soft-sensor, which is a foundation of the proposed control strategy. Also, experiments were carried out to demonstrate the control performance.

4.1 Validation of the feed grade soft-sensor

From the camera sampling system, we selected 316 froth images to extract the features. The data were used to train the FNN. Another 60 groups of data were chosen to validate the feed grade soft-sensor. The initial parameters of the FNN are chosen randomly, and the initial fuzzy sets are determined empirically.

Figure 5 graphs the prediction results of the feed grade soft-sensor. It shows that most of the errors between the

www.manaraa.com

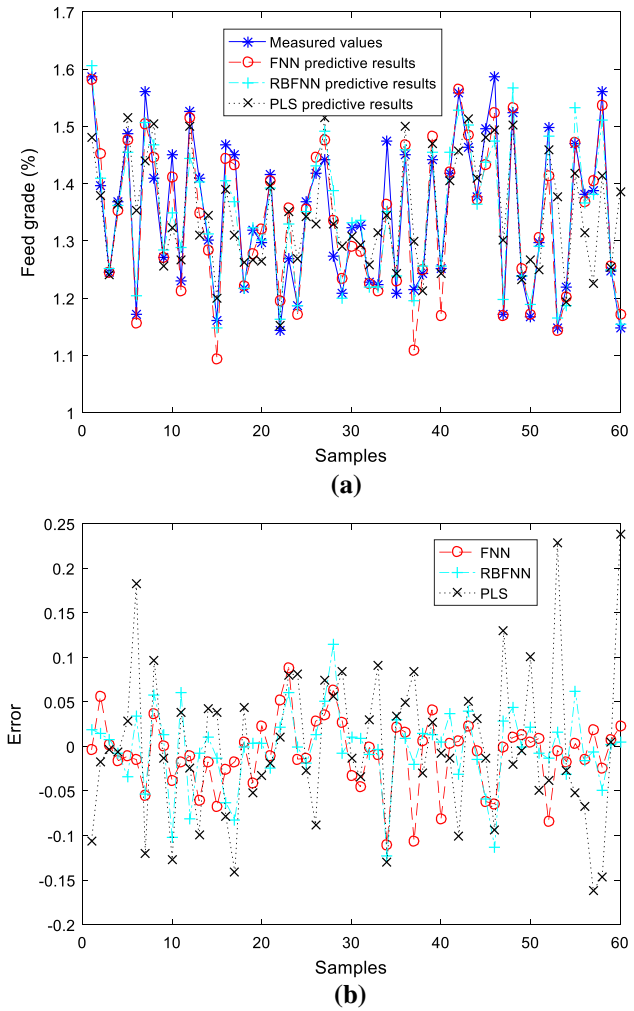

Fig. 5 Prediction comparisons of three different soft-sensors. **a** Predictive results. **b** Predictive errors

predictions of the FNN and the measure feed grades are in the range of [− 0.1, 0.1]. Our proposed FNN-based soft-sensor achieved a good prediction accuracy. To demonstrate the validity and advantages of the proposed feed grade soft-sensor, it is compared with radial basis function neural network (RBFNN) [42] and partial least square (PLS) [43]-based models. The comparison results are presented in Fig. 5. From Fig. 5b, one can conclude that the FNN-based soft-sensor performs best among these three methods. The detailed statistical results from Fig. 5 are summarized in Table 1. Two performance indices are used to evaluate the prediction results, including relative root-mean-square error (RRMSE) and maximum relative error (MRE). The RRMSEs of the FNN and RBFNN are not much different and, however, are better than that of the PLS. The MRE of the FNN-based soft-sensor decreased by 0.3% and 11.96%, respectively, compared with the RBFNN and PLS. Table 1 verifies the effectiveness of the FNN-based soft-sensor.

Table 1 Performance comparisons of three different methods

Methods	RRMSE (%)	MRE (%)
FNN	2.94	8.73
RBFNN	3.03	9.03
PLS	6.55	20.69

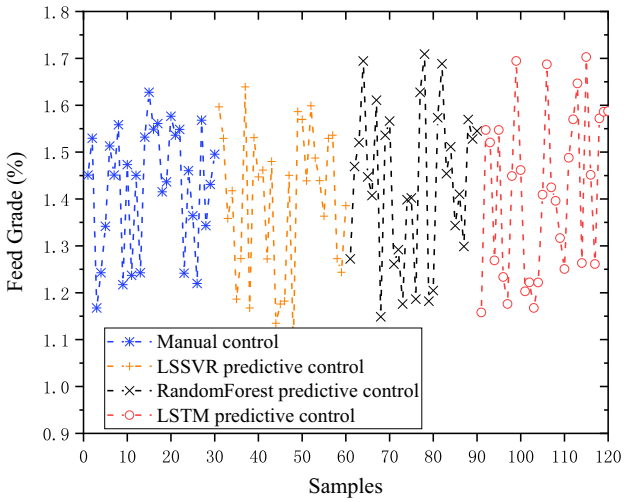

Fig. 6 The feed grade during experiments

4.2 Experiments

The antimony flotation plant in our case is manipulated by operators. Through observing the froth in the rougher bank, the operators adjust the reagent dosages. The concentrate grade is offline assayed every 2 h, which is a time-delay feedback information. The operators will correct their adjustment behavior according to the feedback information.

Every day the plant produces much operational data, in which some are good operations, while some are not. From the numerous operational data, we screen out 1000 groups of data that the concentrate grade is in the desired range. In total, 950 groups of data are used to generate FARs, and the rest are used to validate the results. Then, experiments are conducted to evaluate the proposed optimization and control approach. To demonstrate the validity and advantages of the proposed strategy, our approach is compared with the manual manipulation, least square support vector machine [41], and random forest [44]-based predictive control methods. The feed grade during experiments is presented in Fig. 6. It can be observed that the fluctuation ranges of the feed grade during the manual control and automatic predictive control method are similar, so that a relative fair comparison can be made. The comparison of the control results is described in Figs. 7 and 8. One can conclude that the oscillation range of the concentrate grade using our control approach is narrower than other control

المنارة للاستشارات
www.manaraa.com

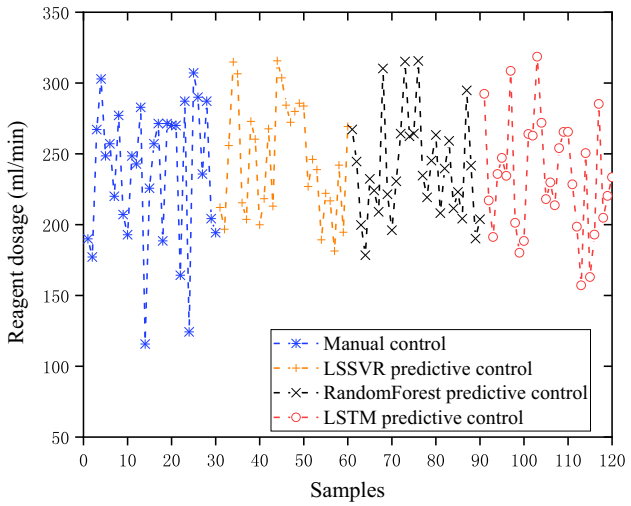

Fig. 7 Control results of the manual operation and our proposed strategy

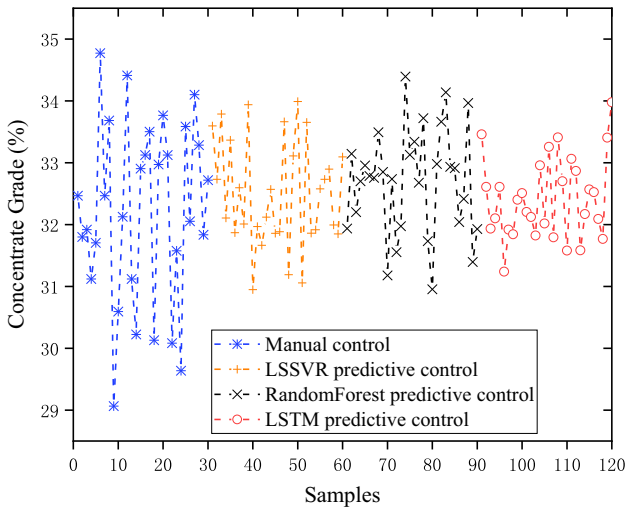

Fig. 8 Control results of the manual operation and our proposed strategy

methods. In further, the proposed strategy controlled more concentrate grade in the desired range, which indicates a better control performance is achieved. More comparisons are summarized in Table 2. The performance indices using in Table 2 include the standard deviation of the concentrate grade (SD) and the oscillation range (OR).

From Table 2, the SD of the concentrate grade with the proposed strategy is improved by 0.81, 0.21, and 0.21, compared with the manual manipulation and other two automatic control methods, respectively. The OR of the concentrate grade is reduced from [29.06%, 34.77%] to [31.24%, 33.98%] compared with the manual manipulation. The results verify the effectiveness of our proposed control strategy. From Figs. 6, 7, and 8, it can be observed that to control the antimony concentrate grade in [31%, 33.5%], reagent dosages should compensate the fluctuation of feed grade promptly. When the feed grade is decreased, the dosage of xanthate should be increased reasonably in time. On the contrary, when the feed grade is increased, the dosage of xanthate should be decreased in time.

Table 2 Comparisons of the control results

Methods	SD	OR
Manual operation	1.47	[29.06%, 34.77%]
LSSVR	0.87	[30.95%, 33.99%]
Random forest	0.87	[30.95%, 34.39%]
Proposed strategy	0.66	[31.24%, 33.98%]

5 Conclusions

In this paper, we propose a FAR-based set-point adaptive optimization and control strategy for the antimony flotation process. The strategy does not require the knowledge of the system dynamics. It consists of three modules: (1) an FNN-based soft-senor to estimate the feed grade online; (2) a FAR-based set-point generator to obtain the optimal set-points of the image features; (3) an LSTM-based predictive controller to track the set-points. Simulations are first carried out to verify the predictive performance of the FNN-based soft-sensor. Then, experiments are conducted to show the performance of the proposed strategy. Compared with manual manipulation, our strategy achieved a better performance, and more concentrate grade is maintained in the desired range.

Acknowledgements This work was supported by the National Science Fund for Distinguished Young Scholars of China (Grant No. 61725306), the National Natural Science Foundation of China (Grant No. 61751312), the Science Fund for Creative Research Groups of the National Natural Science Foundation of China (Grant No. 61621062), and the Fundamental Research Funds for the Central Universities of Central South University (Grant Nos. 2018zzts168 and 2018zzts543).

Compliance with ethical standards

Conflict of interest The authors declare that they have no conflict of interest.

References

1. Chai T, Zhao L, Qiu J, Liu F, Fan J (2013) Integrated network-based model predictive control for setpoints compensation in industrial processes. IEEE Trans Ind Inform 9(1):417–426
2. Xie S, Xie Y, Ying H, Gui W, Yang C (2018) A hybrid control strategy for real-time control of the iron removal process of the zinc hydrometallurgy plants. IEEE Trans Ind Inform 14(12):5278–5288

www.manaraa.com

3. Qiao J, Hou Y, Han H (2017) Optimal control for wastewater treatment process based on an adaptive multi-objective differential evolution algorithm. Neural Comput Appl. https://doi.org/10.1007/s00521-017-3212-4
4. Kaartinen J, Hatonen J, Hyotyniemi H, Miettunen J (2006) Machine-vision-based control of zinc flotation—a case study. Control Eng Pract 14(12):1455–1466
5. Aldrich C, Marais C, Shean BJ, Cilliers JJ (2010) Online monitoring and control of froth flotation systems with machine vision: a review. Int J Miner Process 96(1–4):1–13
6. Liu JJ, MacGregor JF (2008) Froth-based modeling and control of flotation processes. Miner Eng 21(9):642–651
7. Ai M, Xie Y, Xu D, Gui W, Yang C (2018) Data-driven flotation reagent changing evaluation via union distribution analysis of bubble size and shape. Can J Chem Eng 96(12):2616–2626
8. Jahedsaravani A, Marhaban MH, Massinaei M (2014) Prediction of the metallurgical performances of a batch flotation system by image analysis and neural networks. Miner Eng 69:137–145
9. Lawrynczuk M (2011) Online set-point optimisation cooperating with predictive control of a yeast fermentation process: a neural network approach. Eng Appl Artif Intell 24(6):968–982
10. Vega P, Revollar S, Francisco M, Martin JM (2014) Integration of set point optimization techniques into nonlinear MPC for improving the operation of WWTPs. Comput Chem Eng 68:78–95
11. Tang Y, Peng C, Yin S, Qiu J, Gao H, Kaynak O (2014) Robust model predictive control under saturations and packet dropouts with application to networked flotation processes. IEEE Trans Autom Sci Eng 11(4):1056–1064
12. Li J, Chai T, Lewis FL, Fan J, Ding Z, Ding J (2018) Off-policy Q-learning: set-point design for optimizing dual-rate rougher flotation operational processes. IEEE Trans Ind Electron 65(5):4092–4102
13. Xie Y, Wu J, Xu D, Yang C, Gui W (2017) Reagent addition control for stibium rougher flotation based on sensitive froth image features. IEEE Trans Ind Electron 64(5):4199–4206
14. Coenen F, Leng P, Ahmed S (2004) Data structure for association rule mining: T-trees and P-trees. IEEE Trans Knowl Data Eng 16(6):774–778
15. Chen G, Liu H, Yu L, Wei Q, Zhang X (2006) A new approach to classification based on association rule mining. Decis Support Syst 42(2):674–689
16. Alcala-Fdez J, Alcala R, Jose Gacto M, Herrera F (2009) Learning the membership function contexts for mining fuzzy association rules by using genetic algorithms. Fuzzy Set Syst 160(7):905–921
17. Alcala-Fdez J, Alcala R, Herrera F (2011) A fuzzy association rule-based classification model for high-dimensional problems with genetic rule selection and lateral tuning. IEEE Trans Fuzzy Syst 19(5):857–872
18. Kuo RJ, Gosumolo M, Zulvia FE (2017) Multi-objective particle swarm optimization algorithm using adaptive archive grid for numerical association rule mining. Neural Comput Appl. https://doi.org/10.1007/s00521-017-3278-z
19. Sowan B, Dahal K, Hossain MA, Zhang L, Spencer L (2013) Fuzzy association rule mining approaches for enhancing prediction performance. Expert Syst Appl 40(17):6928–6937
20. Sheikhan M, Rad MS (2013) Gravitational search algorithm-optimized neural misuse detector with selected features by fuzzy grids-based association rules mining. Neural Comput Appl 23(7–8):2451–2463
21. Abou SC, Dao T (2009) Fuzzy logic controller based on association rules mining: application to mineral processing. In: Ao SI, Douglas C, Grundfest WS, Burgstone J (eds) Lecture notes in engineering and computer science, Springer, p 878
22. Zhang J, Tang Z, Ai M, Gui W (2018) Fuzzy association rule based froth surface behavior control in zinc froth flotation. Symmetry 10(6):216. https://doi.org/10.3390/sym10060216
23. Astrom KJ, Hagglund T (2001) The future of PID control. Control Eng Pract 9(11):1163–1175
24. Esfandyari M, Fanaei MA, Zohreie H (2013) Adaptive fuzzy tuning of PID controllers. Neural Comput Appl 231:S19–S28
25. Xie S, Xie Y, Huang T, Gui W, Yang C (2019) Generalized predictive control for industrial processes based on neuron adaptive splitting and merging RBF neural network. IEEE Trans Ind Electron 66(2):1192–1202
26. Ying H, Siler W, Buckley JJ (1990) Fuzzy control theory: a nonlinear case. Automatica 26(3):513–520
27. Xie Y, Xie S, Li Y, Yang C, Gui W (2017) Dynamic modeling and optimal control of goethite process based on the rate-controlling step. Control Eng Pract 58(SI):54–65
28. Zheng F, Wang QG, Lee TH (2005) Adaptive robust control of uncertain time delay systems. Automatica 41(8):1375–1383
29. Wu L, Su X, Shi P (2012) Sliding mode control with bounded L2 gain performance of Markovian jump singular time-delay systems. Automatica 48(8):1929–1933
30. Wu L, Zheng WX, Gao H (2013) Dissipativity-based sliding mode control of switched stochastic systems. IEEE Trans Autom Control 58(3):785–791
31. Qin SJ, Badgwell TA (2003) A survey of industrial model predictive control technology. Control Eng Pract 11(7):733–764
32. Abiyev RH (2011) Fuzzy wavelet neural network based on fuzzy clustering and gradient techniques for time series prediction. Neural Comput Appl 20(2):249–259
33. Xie S, Xie Y, Ying H, Jiang Z, Gui W (2020) Neuro-fuzzy-based plant-wide hierarchical coordinating optimization and control: an application to zinc hydrometallurgy plant. IEEE Trans Ind Electron 67(3):2207–2219
34. Ai M, Xie Y, Xie S, Li F, Gui W (2019) Data-driven-based adaptive fuzzy neural network control for the antimony flotation plant. J Frankl Inst 356(12):5944–5960
35. Zhang J, Tang Z, Liu J, Tan Z, Xu P (2016) Recognition of flotation working conditions through froth image statistical modeling for performance monitoring. Miner Eng 86:116–129
36. Ying H (2000) Fuzzy control and modeling: analytical foundations and applications. Wiley-IEEE Press, New York
37. Pizzileo B, Li K, Irwin GW, Zhao W (2012) Improved structure optimization for fuzzy-neural networks. IEEE Trans Fuzzy Syst 20(6):1076–1089
38. Mohanty S (2009) Artificial neural network based system identification and model predictive control of a flotation column. J Process Control 19(6):991–999
39. Cao B, Xie Y, Gui W, Wei L, Yang C (2013) Integrated prediction model of bauxite concentrate grade based on distributed machine vision. Miner Eng 53:31–38
40. Zhang J, Tang Z, Ai M, Gui G (2018) Nonlinear modeling of the relationship between reagent dosage and flotation froth surface image by Hammerstein–Wiener model. Miner Eng 120:19–28
41. Ai M, Xie Y, Xie S, Gui W (2019) Shape-weighted bubble size distribution based reagent predictive control for the antimony flotation process. Chemometr Intell Lab Syst 192:103821
42. Li M, Zhou P, Wang H, Chai T (2019) Geometric analysis based double closed-loop iterative learning control of output pdf shaping of fiber length distribution in refining process. IEEE Trans Ind Electron 66(9):7229–7238
43. Zhao L, Wang D, Chai T (2013) Estimation of effluent quality using PLS-based extreme learning machines. Neural Comput Appl 22(3–4):509–519
44. Smarra F, Jain A, de Rubeis T, Ambrosini D, D'Innocenzo A, Mangharam R (2018) Data-driven model predictive control using

www.manaraa.com

random forests for building energy optimization and climate control. Appl Energy 226:1252–1272

Publisher's Note Springer Nature remains neutral with regard to jurisdictional claims in published maps and institutional affiliations.

www.manaraa.com

Reproduced with permission of copyright owner. Further reproduction prohibited without permission.

www.manaraa.com